Production Rate and Reactivity of Singlet Oxygen 1 O 2 (1 Δ g) Directly Photoactivated at 1270 nm in Lipid Nanocapsules Dispersed in Water

ARTICLE *in* THE JOURNAL OF PHYSICAL CHEMISTRY C · JANUARY 2014

Impact Factor: 4.77 · DOI: 10.1021/jp412497k

THE JOURNAL OF PHYSICAL CHEMISTRY C

Article

pubs.acs.org/JPCC

Production Rate and Reactivity of Singlet Oxygen $^1O_2(^1\Delta_g)$ Directly Photoactivated at 1270 nm in Lipid Nanocapsules Dispersed in Water

A. Sivéry,[†] A. Barras,[‡] R. Boukherroub,[‡] C. Pierlot,[¶] J. M. Aubry,[¶] F. Anquez,[†] and E. Courtade*,[†]

[†]Laboratoire de Physique des Lasers, Atomes et Molécules, UMR 8523, Université Lille Nord de France, Université Lille 1, 59655 Villeneuve d'Ascq, France

[‡]Institut de Recherche Interdisciplinaire (IRI, USR CNRS 3078), Université Lille Nord de France, Université Lille 1, Parc de la Haute Borne, 50 Avenue de Halley, BP 70478, 59658 Villeneuve d'Ascq, France

[¶]Laboratoire de Chimie Moléculaire et Formulation, EA-CMF 4478, Université Lille Nord de France, ENSCL et Université Lille 1, 59655 Villeneuve d'Ascq, France

S *Supporting Information*

ABSTRACT: Singlet oxygen is produced through the O_2 $[^3\sum_g^-] \rightarrow O_2$ $[^1\Delta_g]$ transition of molecular oxygen upon direct 1270 nm laser irradiation in water. The non water-soluble 1,3-diphenylisobenzofuran (DPIBF) is encapsulated in lipid nanocapsules (LNCs) in D_2O and used to monitor the formation of singlet oxygen in these microheterogeneous systems. A two-pseudophase kinetic model for $^1O_2$ distribution is applied to LNCs dispersions in D_2O. From a simple analytical expression of the trap disappearance rate, both the σ_{1270} absorption cross section of the O_2 $[^3\sum_g^-] \rightarrow O_2$ $[^1\Delta_g]$ transition and the reactivity of singlet oxygen toward DPIBF can be evaluated simultaneously and independently in LNCs dispersions in D_2O, and σ_{1270} can be extrapolated to pure deuterated water. The water-soluble chemical trap tetrapotassium rubrene-2,3,8,9-tetracarboxylate (RTC) is used to monitor the formation of singlet oxygen in water and D_2O, and σ_{1270} is also determined in these solvents. Absorption spectrum for the transition O_2 $[^3\sum_g^-] \rightarrow O_2$ $[^1\Delta_g]$ of molecular oxygen is measured in D_2O.

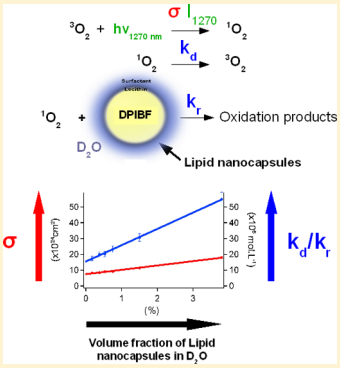

1. INTRODUCTION

Singlet oxygen ($^1O_2$) is the lowest electronic excited state of molecular oxygen (O_2). It is involved in many chemical, photochemical, enzymatical, and biological processes.[1−4] In clinical applications like in photodynamic-therapy,$^1O_2$ is considered as the main cytotoxic agent involved in the eradication of cancer cells.[1,2] Singlet oxygen is generally produced via the use of a photosensitizer (PS), the singlet excited state ^{1}PS* suffers an intersystem crossing, and the excited triplet state ^{3}PS* transfers its energy to molecular oxygen resulting in the formation of various reactive oxygen species (ROS), and in particular singlet oxygen.[5,6] However, $^1O_2$ production via a PS is a complex dynamic system leading to a difficult determination of its direct production rate and reactivity.

In this context, direct excitation of $^3O_2$ has been the focus of several papers.[7−10] Krasnovsky et al. have found that photosensitizer-free 1270 nm high power irradiation (∼1 W) causes photo-oxidation of both tetracene and 1,3-diphenylbenzofuran (DPIBF) at normal temperature and pressure in liquid phases.[8] They have shown that this photo-oxidation process occurs through the reaction of DPIBF with $^1O_2$ produced via the $^3O_2[^3\sum_g^-] \rightarrow {}^1O_2[^1\Delta_g]$ 1270 nm transition.[8−11]

In organic solvents, $^1O_2$ has been investigated using well-known chemical traps: DPIBF, tetracene,[8−11] and rubrene.[12] In a previous paper, we have reported an experimental setup which allows the real-time measurement of DPIBF or rubrene concentration upon 1270 nm laser irradiation in organic solvents and derived a simple analytical expression for the trap consumption rate.[12] Thanks to this expression, the absorption cross section of molecular oxygen (σ_{1270}) for the transition $^3O_2[^3\sum_g^-] \rightarrow {}^1O_2[^1\Delta_g]$ and the reactivity of DPIBF toward singlet oxygen can be determined simultaneously and independently for the studied organic solvents. This chemical trap is highly reactive toward $^1O_2$ but it is not water-soluble (see Figure 1).

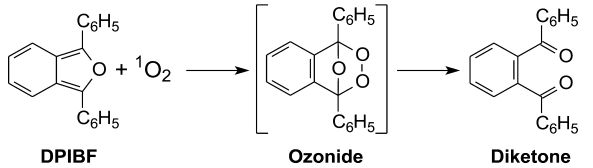

Figure 1. Reaction between DPIBF and $^1O_2$ leading to the formation of an ozonide, which decomposes at room temperature to a diketone.

To characterize $^1O_2$ in the biochemical environment, water-soluble chemical traps or micelles structures should be used to solubilize hydrophobic traps.

Lipid nanocapsules (LNCs) are water-soluble nanocarriers widely investigated for drug delivery and appear to be useful nanostructures for the solubilization of hydrophobic drugs.

Received: December 20, 2013
Revised: January 13, 2014
Published: January 13, 2014

dx.doi.org/10.1021/jp412497k | *J. Phys. Chem. C* 2014, 118, 2885−2893

For example, encapsulation of quercetin in LNCs increases its apparent aqueous solubility by a factor of 100.[13] Also, hypericin (Hy) incorporation into LNCs suppressed its aggregation in aqueous media, increased its apparent solubility, and enhanced the production of singlet oxygen in comparison with free Hy.[14] LNCs are made up of an oily liquid triglyceride core surrounded by a mixed layer of lecithins and a hydrophilic surfactant, which exposes a medium PEG chain containing an average of 15 ethyleneglycol units (see Figure 2). In this study, the non-water-

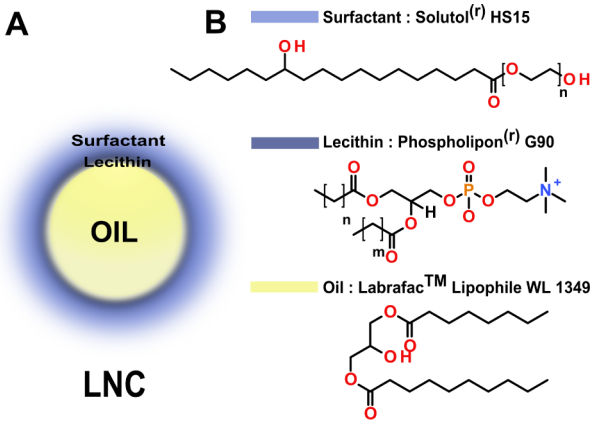

Figure 2. Scheme of lipid nanocapsules. LNCs (~25 nm) are made of a triglyceride core surrounded by a mixed layer of lecithins and a hydrophilic surfactant (~3 nm), which exposes a medium PEG chain containing an average of 15 ethyleneglycol units.

soluble chemical trap DPIBF is encapsulated in LNCs in order to study its reaction kinetics with $^1O_2$ in LNCs dispersions in D_2O and to extrapolate $^1O_2$ production rate to pure deuterated water.

Different water-soluble probes have been synthesized to study singlet oxygen in an aqueous environment.[15−19] An ideal trap for aqueous media should be water-soluble, highly reactive, and specific toward singlet oxygen. The water-soluble trap tetrapotassium rubrene-2,3,8,9-tetracarboxylate (RTC) has been synthetized by Rigaudy and Cuong.[16] The oxidation product formed by reaction between RTC and $^1O_2$ is a stable and colorless endoperoxyde ($RTCO_2$) according to Figure 3. Thus the RTC reaction with singlet oxygen can be monitored by variation of its absorbance around 520 nm.[17] In this study, RTC is used to quantify singlet oxygen production upon 1270 nm laser irradiation in H_2O and D_2O.

2. THEORY

The set of reactions detailed in a homogeneous solution[8−11] is not sufficient to describe the kinetics behavior of $^1O_2$ in microheterogeneous systems. The $^1O_2$ production rate and reactivity are affected by the presence of hydrophilic and hydrophobic compartments. Furthermore, $^1O_2$ distribution equilibrium between aqueous and organic phases needs to be taken into account. A kinetic model for the decay of $^1O_2$ in micellar dispersions has been originally developed by Rodgers et al.[20,21] Thereafter, a two-pseudophase model has been applied to kinetics studies of $^1O_2$ in microemulsions,[22,23] and Martinez et al. have shown that this model was able to predict with good precision both the non-radiative and radiative deactivation rate constants when applied to different types of micellar solutions and microemulsions.[24]

The two-pseudophase model applied to LNCs dispersions in D_2O takes into account that (i) $^3O_2$ absorption cross section (σ_{1270}) for the transition $^3O_2[^3\sum_g^-] \rightarrow {}^1O_2[^1\Delta_g]$ at 1270 nm is different in LNCs and D_2O phases, (ii) $^1O_2$ deactivation rate constant k_d is different in LNCs and D_2O phases, and (iii) the rate constants for $^1O_2$ entry and exit from the LNCs phase are also different. A kinetic scheme related to that proposed by Rodgers et al.[20,21] is displayed in Figure 4.

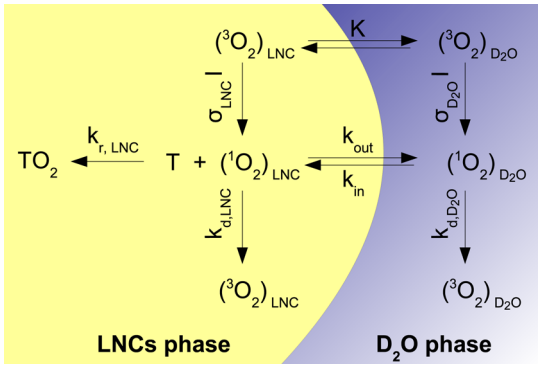

Figure 4. Kinetic scheme of the two-pseudophase model for $^1O_2$ production and deactivation in lipid nanocapsules.

The reactions set for LNCs dispersed in D_2O is given by eq 1 to eq 7:

$$(^3O_2)_{D_2O} + h\nu_{1270} \xrightarrow{\sigma_{D_2O}} (^1O_2)_{D_2O} \quad (1)$$

$$(^3O_2)_{LNC} + h\nu_{1270} \xrightarrow{\sigma_{LNC}} (^1O_2)_{LNC} \quad (2)$$

$$(^1O_2)_{D_2O} \xrightarrow{k_{d,D_2O}} (^3O_2)_{D2O} \quad (3)$$

$$(^1O_2)_{LNC} \xrightarrow{k_{d,LNC}} (^3O_2)_{LNC} \quad (4)$$

$$(^1O_2)_{LNC} + (T)_{LNC} \xrightarrow{k_{q,LNC}} (^3O_2)_{LNC} + (T)_{LNC} \quad (5)$$

$$(^1O_2)_{LNC} + (T)_{LNC} \xrightarrow{k_{r,LNC}} TO_2 \quad (6)$$

$$(^1O_2)_{D_2O} \underset{k_{out}}{\overset{k_{in}}{\rightleftharpoons}} (^1O_2)_{LNC} \quad (7)$$

where $(^3O_2)_x$ is molecular oxygen and $(^1O_2)_x$ singlet oxygen. σ_x is $^3O_2$ absorption cross section for the transition $^3O_2[^3\sum_g^-] \rightarrow {}^1O_2[^1\Delta_g]$ at 1270 nm. $k_{d,x}$ is the rate constant for the quenching of singlet oxygen by the solvent. Then, $k_{d,x} = 1/\tau_{\Delta,x}$ where $\tau_{\Delta,x}$ is

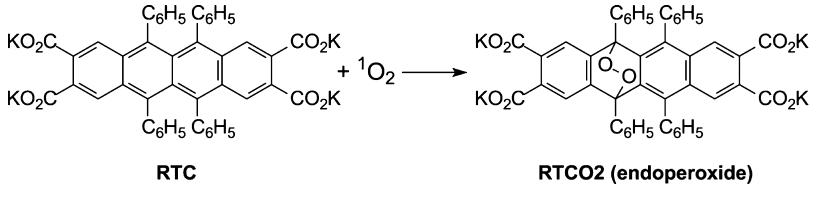

Figure 3. Reaction between RTC and $^1O_2$ leading to the formation of a stable colorless endoperoxide ($RTCO_2$).

dx.doi.org/10.1021/jp412497k | J. Phys. Chem. C 2014, 118, 2885−2893

singlet oxygen lifetime in the absence of trap. x stands for LNC or D_2O phase. k_{in} and k_{out} are the rate constants of $^1O_2$ transfer from one pseudophase to the other. $k_{r,LNC}$ and $k_{q,LNC}$ are the rate constants of singlet oxygen chemical and physical quenching by T in LNC phase, respectively. T is DPIBF and TO_2 is the primary oxidation product formed by reaction between $^1O_2$ and DPIBF.

DPIBF is very reactive toward $^1O_2$, k_r is close to the so-called diffusion limit[3] ($k_r \approx 10^9$ $mol^{-1}\cdot L\cdot s^{-1}$ in micellar aqueous dispersions[25]), and physical quenching k_q is negligible compared to chemical quenching (i.e., $k_q \ll k_r$).[25] Then, the half-quenching concentration β (the so-called "Foote reactivity index") defined by the ratio of singlet oxygen quenching rate constant by the solvent (k_d) on singlet oxygen quenching rate constant by the chemical trap ($k_r + k_q$) is $\beta \approx k_d/k_r$, and eq 5 can be neglected.

Singlet oxygen is directly photoactivated at 1270 nm inside and outside LNCs. Once formed in LNCs, $(^1O_2)_{LNC}$ can be quenched by solvent molecules ($k_{d,LNC}$), reacts with DPIBF ($k_{r,LNC}$) or diffuses out from the nanocapsules (k_{out}). In D_2O phase, $(^1O_2)_{D_2O}$ can be quenched by solvent molecules (k_{d,D_2O}) or reenter the LNCs (k_{in}). The resulting expressions are simplified if one assumes that the equilibrium of $^1O_2$ between the two phases is very fast in comparison with the decay processes, i.e., $k_{in}, k_{out} \gg k_{d,LNC}, k_{d,D_2O}, k_{r,LNC}[T]_{LNC}$. This assumption holds in micellar media where rate constants for entry and exit from micellar aggregates have been reported as not less than $10\ s^{-1}$.[26] compared to $k_d \approx 2.9 \times 10^5\ s^{-1}$ in H_2O.[25] For lipid nanocapsules dispersions, considering a diffusion coefficient (D) for $^3O_2$ of 1.41×10^{-5} $cm^2\ s^{-1}$.[27] and singlet oxygen lifetime in D_2O[28] ($\tau_{\Delta,D_2O} = 68\ \mu s$), the distance traveled by $^1O_2$ (L) over a period (t) of twice its lifetime is ≈ 1069 nm (root-mean-square radial displacement: $L = (6Dt)^{1/2}$.[3,29] Then, the diffusion length of $^1O_2$ is much larger than LNCs mean diameter (~25 nm) and the mean distance between LNCs (~60 to 290 nm for the studied LNCs volume fraction). Thus, an equilibrium is established for $^1O_2$ between the two pseudophases, and the equilibrium constant K_{eq} is given by eq 8:

$$K_{eq} = k_{in}/k_{out} = [^1O_2]_{LNC}/[^1O_2]_{D_2O} \tag{8}$$

where $[^1O_2]_{LNC}$ and $[^1O_2]_{D_2O}$ are $^1O_2$ concentrations in LNC and D_2O phase, respectively.

The kinetic scheme displayed in Figure 4 has been resolved by Lee and Rodgers.[20] In this study, a similar approach has been used with a reactive substrate (T) included in the model as proposed in ref 23. The mean concentration of $^1O_2$ in the mixture, namely, $[^1O_2]$ is given by eq 9 where f_{LNC} and $(1 - f_{LNC})$ are the volume fractions of LNCs and D_2O phases, respectively.

$$[^1O_2] = f_{LNC}[^1O_2]_{LNC} + (1 - f_{LNC})[^1O_2]_{D_2O} \tag{9}$$

Then the time derivative of eq 9 leads to:

$$\frac{d[^1O_2]}{dt} = f_{LNC}\frac{d[^1O_2]_{LNC}}{dt} + (1 - f_{LNC})\frac{d[^1O_2]_{D_2O}}{dt} \tag{10}$$

The rate equations of $^1O_2$ concentration in each pseudophase can be written as follows:

$$\frac{d[^1O_2]_{LNC}}{dt} = \sigma_{LNC}I[^3O_2]_{LNC} - k_{d,LNC}[^1O_2]_{LNC} - k_{r,LNC}[^1O_2]_{LNC}[T]_{LNC} \tag{11}$$

$$\frac{d[^1O_2]_{D_2O}}{dt} = \sigma_{D_2O}I[^3O_2]_{D_2O} - k_{d,D_2O}[^1O_2]_{D_2O} \tag{12}$$

where I is the 1270 nm photon flux which is identical in the two pseudophases.

The relative solubility of $^3O_2$ between the two pseudophases is ruled by the equilibrium constant K where $K = ([^3O_2]_{LNC})/([^3O_2]_{D_2O})$. Furthermore, the equilibrium constant K of $^1O_2$ between the two pseudophases has been shown to be close to the ratio of the solubilities of ground state molecular oxygen in the corresponding alkanes and in water,[24] leading to $K_{eq} \approx K$. Then, considering that $[^3O_2]_{LNC} = K[^3O_2]_{D_2O}$ and $[T] = f_{LNC}[T]_{LNC}$ referring to the substrate concentration in the bulk volume, one can obtain:

$$\frac{d[^1O_2]}{dt} = I[^3O_2]_{D_2O}[f_{LNC}(K\sigma_{LNC} - \sigma_{D_2O}) + \sigma_{D_2O}] - [^1O_2]\frac{[f_{LNC}(Kk_{d,LNC} - k_{d,D_2O}) + k_{d,D_2O}]}{Kf_{LNC} + (1 - f_{LNC})} - [^1O_2][T]\frac{k_{r,LNC}K}{Kf_{LNC} + (1 - f_{LNC})} \tag{13}$$

Microheterogeneous systems like microemulsions can be considered as a homogeneous mixture characterized by apparent rate constants.[23] In LNCs dispersions, the $^1O_2$ reaction rate can also be expressed with apparent rate constant Γ_{app}, $k_{d,app}$, and $k_{r,app}$ referring repectively to $^1O_2$ production rate, the rate constant for the quenching of singlet oxygen by the solvent, and the rate constant of singlet oxygen chemical quenching by T. $^1O_2$ reaction rate can then be expressed as follow:

$$\frac{d[^1O_2]}{dt} = \Gamma_{app} - (k_{d,app} + k_{r,app}[T])[^1O_2] \tag{14}$$

The comparison of eq 13 and eq 14 leads to the apparent (i) $^1O_2$ production rate (eq 15), (ii) $^1O_2$ nonradiative deactivation rate constant by the solvent (eq 16), and (iii) $^1O_2$ chemical quenching with the substrate T (eq 17).

$$\Gamma_{app} = I[^3O_2]_{D_2O}[f_{LNC}(K\sigma_{LNC} - \sigma_{D_2O}) + \sigma_{D_2O}] \tag{15}$$

$$k_{d,app} = \frac{f_{LNC}(Kk_{d,LNC} - k_{d,D_2O}) + k_{d,D_2O}}{Kf_{LNC} + (1 - f_{LNC})} \tag{16}$$

$$k_{r,app} = \frac{k_{r,LNC}K}{Kf_{LNC} + (1 - f_{LNC})} \tag{17}$$

Equation 15 leads to σ_{app}, the apparent absorption cross section for the transition $^3O_2[^3\Sigma_g^-] \rightarrow {}^1O_2[^1\Delta_g]$ at 1270 nm (eq 18).

$$\sigma_{app} = \frac{\Gamma_{app}}{I[^3O_2]_{D_2O}} = [f_{LNC}(K\sigma_{LNC} - \sigma_{D_2O}) + \sigma_{D_2O}] \tag{18}$$

The reactivity index $\beta_{app} = k_{d,app}/k_{r,app}$, which represents the trap concentration at which the quenching of $^1O_2$ by solvent molecules ($k_{d,app}$) equals the decay due to the total quenching by T ($k_{r,app}[T]$), is given by

$$\beta_{app} = \frac{1}{Kk_{r,LNC}}[f_{LNC}(Kk_{d,LNC} - k_{d,D_2O}) + k_{d,D_2O}] \tag{19}$$

Thus, σ_{app} and β_{app} are linear functions of f_{LNC}.

In a solution containing a $^1O_2$ chemical trap upon 1270 nm irradiation conditions, $^1O_2$ production rate $\Gamma_{app} = \sigma_{app}I[^3O_2]_{D_2O}$ ($mol\cdot L^{-1}\cdot s^{-1}$) depends on the 1270 nm photon flux, I ($s^{-1}\cdot cm^{-2}$), on the concentration of dissolved oxygen, $[^3O_2]_{D_2O}$ ($mol\cdot L^{-1}$),

dx.doi.org/10.1021/jp412497k | J. Phys. Chem. C 2014, 118, 2885−2893

and on the absorption cross section σ_{app} (cm^2). As detailed above, the equilibration of $^3O_2$ between the two pseudophases is very fast in comparison with the decay processes of $^1O_2$. Then, the molecular oxygen concentration in the LNCs phase can be considered as constant during the trap photodegradation experiment, and Γ_{app} is only depending on the 1270 nm laser power.

Evolution of the amount of the two different species occurs at two well separated time scales (see ref 12 for details), and quasi-steady-state approximations can be applied to $^1O_2$ leading to eq 20 and to eq 21 for the trap disappearance rate.

$$[^1O_2] = \frac{\Gamma_{app}}{k_{d,app} + k_{r,app}[T]} \quad (20)$$

$$\frac{d[T]}{dt} = -\frac{\Gamma_{app}}{1 + \beta_{app}[T]^{-1}} \quad (21)$$

Two limiting cases can be found for the kinetics of the trap disappearance as detailed in ref 12. At the beginning of the experiment, T is in excess ($[T] \gg \beta_{app}$), then $-d[T]/dt \approx \Gamma_{app}$ is only limited by the $^1O_2$ production rate. When [T] becomes smaller ($[T] \ll \beta_{app}$), one can approximate $-d[T]/dt \approx \Gamma_{app}[T]/\beta_{app}$. For systems trap-solvent in which the inequality $[T_0] \gg \beta$ is verified, values of Γ and β are determined simultaneously and independently. If the inequality is not verified, deviation of the linear regime is not obtained and either Γ or β value can be determined if the other is known. In the case of lipid nanocapsules of DPIBF in D_2O, with an initial concentration of DPIBF ~100 $\mu mol \cdot L^{-1}$, the inequality $[T_0] \gg \beta$ is verified and Γ and β are determined simultaneously and independently. With varying f_{LNC}, the volume fraction of LNCs in D_2O, σ_{app} and β_{app} can be thus determined in LNCs dispersions in D_2O and σ_{1270} can be extrapolated to pure D_2O. In the RTC solutions, the inequality $[T_0] \gg \beta$ is not verified. Then, the analytical expression of $-d[T]/dt = f([T])$ will give a value for Γ if the value of β is constrained to its literature value.[36]

3. EXPERIMENTAL SECTION

DPIBF (1,3-diphenylisobenzofuran, 97%, Sigma Aldrich) is used as received. RTC was synthetized by the laboratory of J. M. Aubry et al. as described in ref 16. For the solvents, distilled water and D_2O (>99.9%, Sigma Aldrich) are used.

3.1. DPIBF Encapsulated in LNCs in D_2O. *Materials.* Lipid nanocapsules are made of Labrafac Lipophile WL 1349 (caprylic/capric triglyceride), Phospholipon 90G (soybean lecithin at 97.1% of phosphatidylcholine), and Solutol HS15 (a mixture of free polyethylene glycol 660 and polyethylene glycol 660 hydroxystearate) generously provided by Gattefosse S.A.S. (Saint-Priest, France), Phospholipid GmbH (Köln, Germany), and Laserson (Etampes, France), respectively. Deionized water is obtained from a Milli-Q plus system (Millipore, Paris, France). Other chemical reagents and solvents are obtained from Sigma-Aldrich (Saint-Quentin Fallavier, France) and used as received.

Preparation of DPIBF-Loaded LNCs. LNCs are formulated at a nominal size of 25 nm in D_2O using a phase inversion method of an oil/water system, as described by Heurtault.[30] Briefly, the oil phase containing Labrafac (252 mg) and Phospholipon 90G (37.5 mg) is mixed with the appropriate amounts of Solutol (408 mg), D_2O (540 μL), and NaCl (44 mg), and heated under magnetic stirring up to 80 °C. The mixture is subjected to 2−3 temperature cycles from 40 to 70 °C under magnetic stirring. Then, it is cooled to 55 °C, 3.3 mL of cold D_2O (0 °C) are added, and the suspension (4.2 mL) is still stirred at room temperature in the dark for another 10 min before further use. DPIBF-loaded LNCs are prepared using two distinct methods. For low DPIBF amounts (<1% oily phase), DPIBF is solubilized in acetone (10 mg/mL). Then, the heating cycles are operated and the appropriate volumes of DPIBF solution are introduced at the beginning of the last cooling. For high DPIBF amounts (>1% oily phase), DPIBF is directly dissolved in the oily phase and the heating cycles are realized. Then, DPIBF-loaded LNCs are purified using a disposable PD-10 desalting column (Sephadex G-25 for gel filtration as stationary phase, Amersham Biosciences). The column is stabilized with 25 mL of D_2O. Then 2 mL of LNC suspensions are deposited on the column, 0.5 mL of D_2O are added to complete the dead volume of the column, then 4 mL of D_2O eluted and the purified LNCs are collected in this eluant (dilution factor of gel filtration = 2). The volume of LNCs is estimated to be ~0.63 ± 0.06 mL in 8.4 mL of purified suspensions. Thus, for this initial formulation, the volume fraction of LNCs in D_2O ($f_{LNC} = V_{LNC}/(V_{LNC} + V_{D_2O})$ where V_{LNC} and V_{D_2O} are the volume of LNCs and D_2O, respectively) is ~0.075.

DPIBF loading. The DPIBF loading of purified LNC suspensions is directly determined by reversed phase-high performance liquid chromatography (RP-HPLC). RP-HPLC analyses are performed on a Shimadzu LC2010-HT instrument (Shimadzu, Tokyo, Japan). A 5 μm C4 QS Uptisphere 300 Å, 250 × 4.6 mm column (Interchim, Montluçon, France) is used as the analytical column. The column is heated to 40 °C. The mobile phase is a mixture of eluent A (trifluoroacetic acid 0.05% in H_2O) and eluent B (trifluoroacetic acid 0.05% in CH_3CN) at a flow rate of 1 mL/min. The linear gradient is 0% to 80% of eluent B in 30 min, and detection is performed at 410 nm. A 10 mM stock solution of DPIBF is prepared in dimethylsulfoxide for the calibration curve. Concentrations of 10−100 μM of DPIBF in dimethylsulfoxide are prepared from this stock. Each sample is injected (40 μL) into the RP-HPLC column. Calibration curves (y = 54872x, r = 0.9999) are obtained by linear regression of DPIBF concentration (x, μM) versus the peak area (y).

3.2. Experimental Setup. We set up an experiment to perform kinetics measurements of the trap concentration in a solution irradiated with a 1270 nm laser.[12]

Reaction of $^1O_2$ with DPIBF (or RTC) leads to colorless oxidation products. Thus the trap concentration can be monitored via the 410 nm band of DPIBF, or the 520 nm band of RTC (see Figure 5) by measuring the absorbance of the solution. Using a spectrometer (Perkin-Elmer, lambda 19) we have verified that normalized absorption spectra of DPIBF (and RTC) before and after 1270 nm irradiation superimpose almost perfectly in the visible range (data not shown). This means that the oxidized products of the reaction does not induce any shift or distortion in the visible part of the spectrum. A 405 nm (532 nm) laser whose wavelength matches the DPIBF (RTC) absorption spectrum is used to measure the trap absorbance in the solution. Values of $\varepsilon_{405} \approx 17.70 \times 10^3$ $L \cdot mol^{-1} \cdot cm^{-1}$ and $\varepsilon_{532} \approx 7.42 \times 10^3$ $L \cdot mol^{-1} \cdot cm^{-1}$ are calculated for the molar absorption coefficient of DPIBF and RTC, respectively, in water and D_2O. Measurements of ε_{405} (ε_{532}) using either the 405 nm (532 nm) laser or the spectrometer give consistent results.

A scheme of the experimental setup is displayed in Figure 6. Solutions of DPIBF-loaded LNCs or RTC (~120 $\mu mol \cdot L^{-1}$) are placed in a quartz cell of 1 × 1 × 5 cm^3 (Hellma). The volume of the solutions is 1.4 mL. Fresh DPIBF-loaded LNCs dispersions and RTC solutions are stocked in the dark, at room temperature. Pure oxygen is bubbled using a thin pasteur pipet inside RTC solutions at least 1 h before irradiation in order to increase the

dx.doi.org/10.1021/jp412497k | J. Phys. Chem. C 2014, 118, 2885−2893

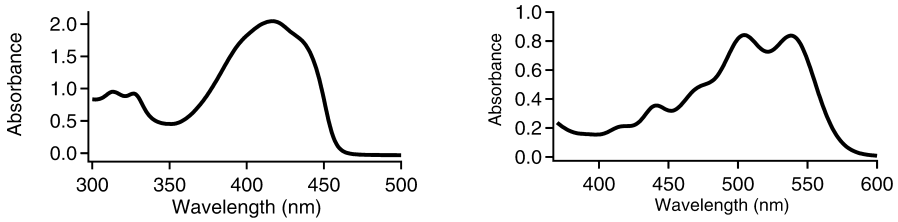

Figure 5. Absorption spectra in D_2O of (a) DPIBF-loaded LNCs with $[T_0] = 120\ \mu mol{\cdot}L^{-1}$ for $f_{LNC} = 0.015$ and (b) RTC with $[T_0] = 110\ \mu mol{\cdot}L^{-1}$ using a spectophotometer.

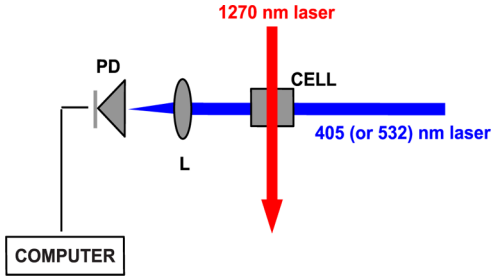

Figure 6. Scheme of the experimental setup for measurement of DPIBF-loaded LNCs or RTC consumption rate upon 1270 nm excitation of $^3O_2$.[31] The trap concentration is monitored by a 405 nm (532 nm) laser beam for DPIBF (RTC), focused on a photodiode (PD) by a lens (L). The 1270 nm and the 405 nm (532 nm) lasers intersect in the quartz cell containing DPIBF-loaded LNCs dispersions (RTC solutions) saturated with air and oxygen, respectively.

amount of dissolved oxygen and the rate of reaction between RTC and $^1O_2$. During all the duration of the experiment, the oxygen blowing is maintained above the liquid phase in order to saturate the solutions in $^3O_2$. As the rate of reaction is high enough in DPIBF-loaded LNCs, no bubbling is performed, and these solutions are saturated with air.

Two lasers are used: a Raman fiber ring laser operating at 1270 nm[31] for $^1O_2$ production and a laser emitting at 405 nm or 532 nm for the monitoring of DPIBF or RTC concentration, respectively. These two laser beams are perpendicular and intersect in the quartz cell. The diameter of the infrared beam irradiating the quartz cell is ~3 mm with a power ~1 W measured with a power meter (Ophir). The beam diameter of laser which monitors [T] is adjusted to ~8 mm in order to homogeneously cover all the section of the solution. To prevent photobleaching of the trap, the laser power is reduced down to a power of ~10 μW and is switched using a mechanical shutter opened for ~5 s every 5 min. Irradiations last for ~8 h in D_2O. The whole set up is covered to avoid bleaching of the solutions with daylight. Several experiments have been performed in DPIBF-loaded LNCs dispersions (RTC solutions) without 1270 nm irradiation in D_2O and H_2O: no variation of 405 nm (532 nm) absorbance is detected for as long as 8 h (data not shown). This confirms that the trap disappearance results only from the 1270 nm irradiation.

4. RESULTS AND DISCUSSION

4.1. Rate of $^1O_2$ Production and Reactivity with DPIBF in LNCs Dispersions in D_2O. DPIBF is a trap of choice to evaluate singlet oxygen production rate and reactivity because of its high reactivity toward singlet oxygen.[8−12] But because of its nonsolubility in water, its use has been strictly limited to organic solvents or micellar media.[8,10,11]

Our analytical expression of the trap disappearance rate is of great interest for solutions where the inequality $[T_0] \gg \beta$ is verified. In these conditions, σ and β are determined simultaneously and independently. In D_2O, we choose to use LNCs in which DPIBF is encapsulated in order to determine σ_{app} and β_{app} in LNCs dispersions in D_2O. The volume fraction of LNCs (f_{LNC}) dissolved in D_2O is in the range of 0.17% to 3.8% in order to determine σ_{app} and β_{app} (i) in LNCs dispersions in D_2O and (ii) to extrapolate σ_{1270} to pure D_2O.

DPIBF is encapsulated in LNCs at around 100 μM and irradiated with the Raman fiber ring laser[31] at 1270 nm at the power of ~1 W. The 1270 nm absorption in D_2O induces a temperature increase. In this solvent, singlet oxygen lifetime and dissolved molecular oxygen concentration decrease with the temperature.[32,33] At a typical laser power of 1 W, an elevation temperature of ~6 °C has been measured leading to $\tau_{\Delta,D_2O} = 66\ \mu s$ and $[^3O_2]_{D_2O} = 2.46 \times 10^{-4} mol{\cdot}L^{-1}$. Figure 7 (a) shows the decrease of DPIBF concentration for $[T_0] = 124\ \mu mol{\cdot}L^{-1}$ in D_2O at $f_{LNC} = 0.0017$ upon 1270 nm irradiation at ~1.1 W.

Modelization of the ordinary differential equations for singlet oxygen and the trap is performed to confirm the validity of our analytical expression of the trap disappearance rate (eq 21) and the obtained values of Γ_{app} and β_{app}. The least-squares method is applied to the evolution of the trap concentration over time (t): $[T] = f(t)$ (see Figure 7a), and from the best fit of the experimental data, values of $\Gamma_{app} = 7.95 \times 10^{-9}\ mol{\cdot}L^{-1}{\cdot}s^{-1}$ and $\beta_{app} = 17.3 \times 10^{-6}\ mol{\cdot}L^{-1}$ are obtained.

The trap disapperance rate as a function of [T] for the same experiment is represented in Figure 7b. A reliable fit of the data is obtained using the following expression:

$$-\frac{d[T]}{dt} = \frac{a}{1 + b[T]^{-1}} \tag{22}$$

where $a = \Gamma_{app}$ and $b = \beta_{app}$.

Singlet oxygen production rate Γ_{app} and the reactivity index β_{app} are unambiguously determined by parameters a and b, respectively. Values of $a = 7.98 \times 10^{-9}\ mol{\cdot}L^{-1}{\cdot}s^{-1} \pm 3\%$ and $b = 17.5 \times 10^{-6}\ mol{\cdot}L^{-1} \pm 9\%$ are obtained. The values obtained for Γ_{app} and β_{app} with the two methods are in really good agreement, confirming the accuracy of the analysis of the trap disappearance rate (eq 21).

The average 1270 nm photon flux is

$$I = \frac{P_0 L}{h\nu V_{sol}}\left(\frac{1 - e^{-\alpha L}}{\alpha L}\right)K_{quartz} \tag{23}$$

in $s^{-1}{\cdot}cm^{-2}$, where $P_0 = 1.1\ W \pm 1\%$ is the laser power and $L = 1$ cm is the length of the quartz cuve, $h\nu$ is the energy of 1270 nm photons, $V_{sol} = 1.4$ mL is the volume of the solution in the cell, α is the linear absorption coefficient at 1270 nm of the solvent, due to inactive absorption of laser light which is ~0.17 cm^{-1} in LNCs

dx.doi.org/10.1021/jp412497k | J. Phys. Chem. C 2014, 118, 2885−2893

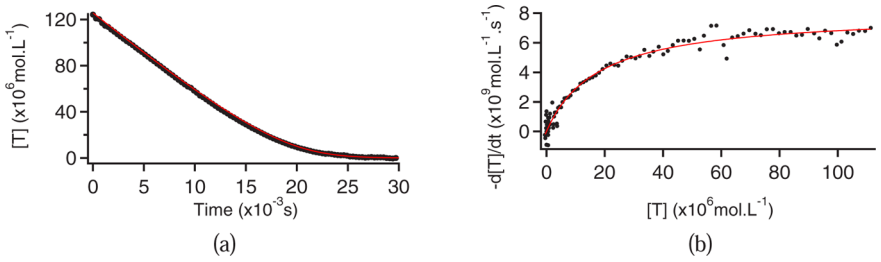

Figure 7. (a) Experimental evolution of DPIBF encapsulated in LNCs dispersed in D_2O for $[T_0] = 124\ \mu mol{\cdot}L^{-1}$ with $f_{LNC} = 0.0017$ upon 1270 nm irradiation at a power of 1.1 W (dots). Modelization of the equation set is performed, and from the best fit (solid line) of the experimental data the values of $\Gamma_{app} = 7.95 \times 10^{-9}\ mol{\cdot}L^{-1}{\cdot}s^{-1}$ and $\beta_{app} = 17.3 \times 10^{-6}\ mol{\cdot}L^{-1}$ are obtained. (b) Disappearance rate of DPIBF with $f_{LNC} = 0.0017$ in D_2O as a function of [T] (dots). A best fit of the experimental data is performed (solid line) through eq 22, parameters $a = 7.98 \times 10^{-9} mol{\cdot}L^{-1}{\cdot}s^{-1} \pm 3\%$ and $b = 17.5 \times 10^{-6}\ mol{\cdot}L^{-1} \pm 9\%$ are obtained.

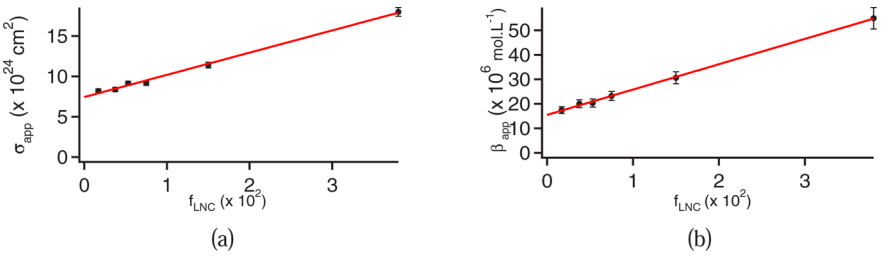

Figure 8. Evolution of σ_{app} (a) and β_{app} (b) as a function of the volume fraction of LNCs dispersed in D_2O for $0.17 < f_{LNC} < 3.8\%$. The slopes of the curves are $275 \times 10^{-24}\ cm^2 \pm 3\%$ and $1034 \times 10^{-6}\ mol{\cdot}L^{-1} \pm 2\%$ for $\sigma_{app} = f(f_{LNC})$ and $\beta_{app} = f(f_{LNC})$ respectively. σ_{1270} can be then extrapolated to pure D_2O. A value of $\sigma_{D_2O} = 7.4 \times 10^{-24}\ cm^2 \pm 2\%$ is obtained. For $f_{LNC} = 0$, $\beta_{app} = 15.5 \times 10^{-6}\ mol{\cdot}L^{-1} \pm 2\%$ is found.

dispersions in D_2O and in pure D_2O, and ~1.09 cm^{-1} in H_2O. K_{quartz} (~0.94) is the absorption of laser light by the first side of the quartz cell.

Thanks to eq 23, with a value of $\Gamma_{app} = 7.98 \times 10^{-9}\ mol{\cdot}L^{-1}{\cdot}s^{-1}$, a value of $\sigma_{app} = 8.2 \times 10^{-24}\ cm^2 \pm 4\%$ is obtained for $f_{LNC} = 0.0017$.

DPIBF-loaded LNCs dispersions in D_2O have been analyzed by HPLC measurement before and after 1 h and 2 h irradiations at 1270 nm. Two oxidation products of reaction between $^1O_2$ and DPIBF have been identified. DPIBF leakage during irradiation is constant and low (~10%) (see Supporting Information). The reaction between $^1O_2$ and DPIBF must have occurred mainly inside LNCs or at the interface between LNCs and D_2O phases. To assess the solvent effect on $^1O_2$ reactivity toward DPIBF in LNCs dispersions, we have performed experiments at the same LNCs volume fraction of 0.0017 in D_2O and H_2O. DPIBF disappearance rate is highly increased in D_2O compared to H_2O, reflecting relative singlet oxygen lifetimes in the two solvents (see Supporting Information).

Therefore, singlet oxygen is produced inside and outside LNCs, but reaction between $^1O_2$ and DPIBF must occur inside LNCs or at the interface between LNCs and D_2O phases. The kinetic scheme depicted in section 2 is thus in agreement with these experimental observations.

4.2. Influence of LNCs Volume Fraction on $^1O_2$ Production Rate and Reactivity with DPIBF. To evaluate the complexity of the environment on $^1O_2$ production rate and reactivity with DPIBF, the concentration of LNCs in D_2O has been varied. The volume fraction of LNCs is set between 0.17% and 3.8%. Figure 8 shows the evolution of σ_{app} (a) and β_{app} (b) with the volume fraction of LNCs. σ_{app} and β_{app} vary linearly with the volume fraction of LNCs for f_{LNC} up to 3.8%.

Experiments on empty LNCs have been performed to assess the effect of 1270 nm irradiation on their stability. Both absorbance and DLS measurements reveal that no LNCs damages are observed upon 1270 nm laser irradiation for $0.17\% < f_{LNCs} < 3.8\%$ (see Supporting Information).

The linear increase of $^1O_2$ production with f_{LNC} could be explained by a higher absorption cross section and a higher solubility of oxygen in the LNCs phase compared to the D_2O phase. In fact the LNCs core is made of an oily liquid triglyceride core, and oxygen solubility is increased by a factor ~4 between water and olive oil.[34] The reactivity index β_{app} also increases linearly with f_{LNC}, corresponding to a decrease of the apparent $^1O_2$ lifetime $\tau_{\Delta,app}$ and a decrease of $k_{r,app}$. In complex environments, quenching of singlet oxygen by surrounding molecules is expected to increase, resulting in a smaller singlet oxygen lifetime. For example τ_Δ is decreasing with increasing SDS concentration in D_2O.[24] Finally the reactivity between DPIBF and singlet oxygen may decrease due to greater viscosity of solutions as proposed in ref 10.

On the basis of the expression proposed in section 2 for the behavior of σ_{app} with f_{LNC}, values of σ_{D_2O} and σ_{LNC} can be extrapolated at $f_{LNC} = 0$ and $f_{LNC} = 1$, respectively. The slope of the curve $\sigma_{app} = f(f_{LNC})$ is equal to $275 \times 10^{-24}\ cm^2 \pm 3\%$ corresponding to $K\sigma_{LNC} - \sigma_{D_2O}$. With a value of $K \approx 4$[34] and $\sigma_{D_2O} = 7.4 \times 10^{-24}\ cm^2 \pm 2\%$, a value of $\sigma_{LNC} = 71 \times 10^{-24}\ cm^2 \pm 3\%$ is obtained.

Through the changes of β_{app} with f_{LNC}, values of $k_{r,LNC}$ and $k_{d,LNC}$ can be determined. A value of $\beta_{app} = 15.5 \times 10^{-6}\ mol{\cdot}L^{-1} \pm 2\%$ is found at $f_{LNC} = 0$. Then considering $k_{d,D_2O} = 1.5 \times 10^4\ s^{-1} \pm 4\%$,[28] a value of $k_{r,LNC} = 2.44 \times 10^8\ mol^{-1}{\cdot}L{\cdot}s^{-1} \pm 6\%$ is obtained. From the slope of the curve $1034 \times 10^{-6}\ mol{\cdot}L^{-1} \pm 2\%$, a value of $k_{d,LNC} = 2.56 \times 10^5\ s^{-1} \pm 8\%$ is obtained.

Through the increase of β_{app} with f_{LNC}, the decrease of $\tau_{\Delta,app}$ with f_{LNC} is revealed (see Figure 9). In fact, $\tau_{\Delta,app}$ can be expressed as follows:

$$\tau_{\Delta,app} = \frac{1}{\beta_{app} k_{r,app}} = \frac{1}{\beta_{app}} \frac{K f_{LNC} + (1 - f_{LNC})}{K k_{r,LNC}} \quad (24)$$

dx.doi.org/10.1021/jp412497k | J. Phys. Chem. C 2014, 118, 2885−2893

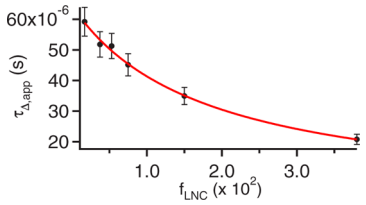

Figure 9. Apparent $^1O_2$ lifetime as a function of f_{LNC} in LNCs dispersions in D_2O (black dots (eq 24) and red straight line (eq 16)). $\tau_{\Delta,app}$ decreases from 66 μs in pure D_2O, to 21 μs in LNCs dispersions in D_2O at f_{LNC} = 0.038 due to the increase of the environment complexity.

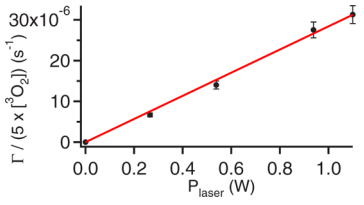

Figure 10. Production rate of singlet oxygen in D_2O as a function of the infrared laser power. RTC solutions saturated with oxygen in D_2O are irradiated upon 1270 nm at different laser power ranging from 0.3 to 1.2 W. From a linear fit, the slope of the curve $(2.84 \times 10^{-5} \pm 5.63 \times 10^{-7})s^{-1}$ is obtained, and then one can evaluate $\sigma_{D_2O} = 7.2 \times 10^{-24}$ cm^2 ± 3%.

We have performed an irradiation experiment at 1270 nm in pure Labrafac, the triglyceride making up the core of LNCs. From the trap disappearance rate, a value of $\sigma_{labrafac} \approx 68 \times 10^{-24}$ cm^2 has been found and in good agreement with σ_{LNC}. A value of $\beta_{labrafsc} \approx 250 \times 10^{-6}$ mol·L^{-1} has been also estimated, which is four times lower than β_{LNC}, indicating that $^1O_2$ deactivation in LNCs takes place both in the oily core and in the mixed layer of lecithins and the hydrophilic surfactant.

4.3. $^1O_2$ Production Rate in Pure D_2O and H_2O. Values of σ_{D_2O} can be extrapolated at LNCs concentration equals zero (see Figure 8). In order to confirm the extrapolated value of $\sigma_{D_2O} = 7.4 \times 10^{-24}$ cm^2 ± 2%, the water-soluble chemical trap RTC has been used.

RTC solutions around 100 μM are irradiated with the Raman fiber ring laser (~1 W).[31] Postulating $\beta_{D_2O} = 1.01 \times 10^{-4}$ mol^{-1}·L·s^{-1},[17,28] a mean value of $\sigma_{D_2O} = 6.8 \times 10^{-24}$ cm^2 ± 16% is obtained in which the uncertainty is a standard deviation upon 10 experiments. Then the values found with RTC and with DPIBF-loaded LNCs for $f_{LNC} = 0$ are in good agreement with those in ref 36. One can notice that, if β is set free in the best fit of the curve $[T] = f(t)$, values of $\sigma_{D_2O} = 7.6 \times 10^{-24}$ cm^2 ± 51% and $\beta_{D_2O} = 9.5 \times 10^{-5}$ mol^{-1}·L·s^{-1} ± 49% are obtained. The uncertainties clearly show that σ and β cannot be determined independently in the case of RTC where $[T_0] \approx \beta$. Otherwise the mean value of β_{D_2O} is in excellent agreement with the value of that in 36.

To test the influence of dissolved oxygen concentration on the production rate of singlet oxygen, we have also performed experiments with RTC solutions satured with air and nitrogen as in refs 12, 37 and 38. For the solution satured with nitrogen, no degradation of RTC has been observed for 1 h of 1270 nm irradiation at 1 W. The singlet oxygen production rate is multiplied by a factor ~5 for the solution saturated with oxygen compared to the solution saturated with air (see Supporting Information for details). Moreover, we have conducted control experiments which confirm that oxidation products do not affect RTC disappearance kinetics (see Supporting Information).

The case of H_2O is probably the most interesting because of the involvement of $^1O_2$ in the oxidation process in biological systems.[39−41] Experiments in RTC solutions in H_2O have been performed leading to a mean value of $\sigma_{h_2o} = 7.6 \times 10^{-24}$ cm^2 ± 4% where the uncertainties are standard deviations upon three experiments. Then this value is in good agreement with the extrapolated value of 7.2 × 10^{-24} cm^2 found when SDS concentration approaches zero in H_2O.[10] The values found for σ_{1270} in H_2O and D_2O are similar.

4.4. Heating Effect on $^1O_2$ Production Rate in D_2O. To evaluate heating effects on the trap disappearance kinetics, RTC solutions saturated with oxygen in D_2O are irradiated at 1270 nm at different laser power, ranging from 0.3 to 1.2 W. From a best fit of the curve $[T] = f(t)$, Γ is obtained for each experiment. For the analysis, a value of k_r = 1.5 × 10^8 mol^{-1}·L·s^{-1}.[17] is hypothetized and $^1O_2$ lifetimes are calculated in order to take into account the increase of temperature due to IR laser. Figure 10 exhibits singlet oxygen production rate as a function of the 1270 nm laser power. From the slope of the curve (see section 2) a value of $\sigma_{D_2O} = 7.2 \times 10^{-24}$ cm^2 ± 3% is determined, which is in good aggrement with the mean value of σ_{D_2O} found in section 4.3. Thus, the heating of RTC solutions in D_2O does not seem to affect the production rate of singlet oxygen. Moreover, σ_{D_2O} is in very good agreement with the values obtained in section 4.3 (see Table 1).

Table 1. Summary of the Obtained Values for σ_{1270} in H_2O, D_2O, and LNCs[a]

solvents	H_2O	D_2O
σ_{1270} (10^{-24} cm^2)	7.6 ± 4%[b]	7.4 ± 2%[a]
		7.6 ± 51%[b]
		7.2 ± 3%[c]
	7.2[10]	9.17[35]
σ_{LNC} (10^{-24} cm^2)		71 ± 3%[a]
$k_{r,LNC}$ (10^8 mol^{-1}·L·s^{-1})		2.44 ± 6%[a]
$k_{d,LNC}$ (10^5 s^{-1})		2.56 ± 8%[a]
β_{RTC} (10^{-5} mol·L^{-1})		9.5 ± 49%[b]
		9[36]

[a]Rate constants of $^1O_2$ chemical quenching by DPIBF ($k_{r,LNC}$) and quenching by the solvent ($k_{d,LNC}$) in LNCs as well as the reactivity index β_{RTC} in H_2O are reported. Values obtained with DPIBF-loaded LNCs dispersions in D_2O (a), RTC solutions (b), and with varying the 1270 nm laser power in RTC solutions in D_2O (c). Published values are reported from refs 10, 35, and 36.

Concerning β we have not observed any dependence with the temperature. C.A. Long and D.R. Kearns have studied the evolution of k_r with the temperature in DPIBF solutions of $CHCl_3$ and observed a decrease of 6% for k_r with an increase of temperature of 10 °C.[42] They emit the hypothesis of a dependence of k_r with the temperature related to change in viscosity of $CHCl_3$ with temperature. If one considers the viscosity dependence of D_2O with temperature, a decrease of 22% is observed between 20 and 30 °C.[3] Then regarding the uncertainty of β, our study does not allow a conclusion of any possible effect for RTC reactivity toward singlet oxygen with the temperature.

4.5. Absorption Spectrum of the Transition $^3O_2[^3\sum_g^-] \rightarrow {}^1O_2[^1\Delta_g]$ of Molecular Oxygen in D_2O. Absorption maximum of the transition $^3O_2[^3\sum_g^-] \rightarrow {}^1O_2[^1\Delta_g]$ of molecular oxygen is known to depend on the surrounding environment. Compared to the gas phase, the absorption maximum is shifted to the red in solvents.[43] An effect on the shape of the band for absorption or emission have also been observed in some solvents.[42,44] The

dx.doi.org/10.1021/jp412497k | J. Phys. Chem. C 2014, 118, 2885−2893

wavelength shift depends on the refractive index of solvent and then on the polarizability of solvent molecules.[45] Bromberg et al. have measured a shift of 6 nm for the emission maximum of the transition $^1O_2[^1\Delta_g]$ $^3O_2[^3\sum_g^-]$ between acetone (λ_{em} = 1273 nm) and anisole (λ_{em} = 1279 nm).[46]

To determine the location of the absorption maximum for the transition $^3O_2[^3\sum_g^-] \rightarrow {}^1O_2[^1\Delta_g]$ of molecular oxygen, we have performed irradiation of RTC solutions in D_2O between 1247 and 1288 nm at the same IR power. From a best fit of the curves [T] = $f(t)$, the absorption cross section of molecular oxygen is determined for each wavelength.

Figure 11 represents the normalized absorption cross section for the transition $^3O_2[^3\sum_g^-] \rightarrow {}^1O_2[^1\Delta_g]$ of molecular oxygen as a function of the irradiation wavelength. The absorption maximum is ∼1273 nm ± 1 nm and the full width at half-maximum is 18 nm ± 2 nm. The same experiments have been performed previously with DPIBF solutions in acetone and ethanol.[31] No significant difference is found between D_2O and the tested organic solvents on the absorption maximum or on the shape of the absorption band. In ref 46, the shift between CD_3OD (whose refractive index (n = 1.329) is close to that of D_2O (n = 1.3284) and acetone d_6 ($n \approx 1.35$) is only 1 nm. Considering the uncertainty on the absorption maximum location and the slight difference in the refractive index between D_2O and acetone−ethanol, our results are quiet consistent.

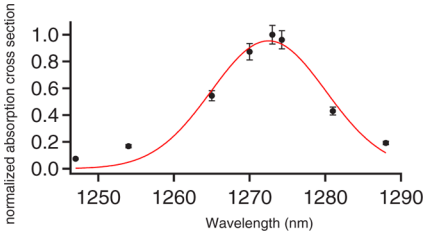

Figure 11. Normalized absorption cross section of molecular oxygen for the transition $^3O_2[^3\sum_g^-] \rightarrow {}^1O_2[^1\Delta_g]$ as a function of wavelength in D_2O. RTC solutions of ∼100 μM in D_2O are irradiated between 1247 and 1288 nm at the same laser power. From a best fit of the curve [T] = $f(t)$, the absorption cross section is evaluated at each wavelength.

5. CONCLUSION

An experimental setup combined with a simple analytical expression of the trap disappearance rate is used to determine, in water, the production rate of singlet oxygen and its reactivity with a chemical trap, upon direct excitation at 1270 nm.

In dispersions of DPIBF-loaded LNCs, the analysis of the trap disappearance rate enables the simultaneous and independent determination of singlet oxygen production rate and reactivity with DPIBF in dispersions of LNCs in D_2O and extrapolated σ_{1270} to pure D_2O. The complexity of the environment on $^1O_2$ production rate and reactivity with DPIBF is studied with a varying concentration of LNCs in D_2O. σ_{app} and β_{app} increase linearly with the volume fraction of LNCs for f_{LNC} up to 3.8%. A two-pseudophase kinetic model is able to describe the behavior of σ_{app} and β_{app} with the volume fraction of LNCs. The value extrapolated for σ_{D_2O} at zero LNCs concentration is close to the expected values in pure deuterated water.[35] The absorption spectrum of molecular oxygen for the transition $^3O_2[^3\sum_g^-] \rightarrow {}^1O_2[^1\Delta_g]$ has been measured in D_2O. The maximum of the absorption and the width of the band are quiet similar with those previously obtained in acetone and ethanol.[31]

The water-soluble chemical trap RTC is used for its high specificity and reactivity toward singlet oxygen.[17,36] In water and D_2O, the absorption cross section of molecular oxygen for the transition $^3O_2[^3\sum_g^-] \rightarrow {}^1O_2[^1\Delta_g]$ at 1270 nm has been measured and is in good agreement with the published values.[10,35] Unfortunately, the reactivity of RTC is too small to enable the simultaneous determination of σ_{1270} and the reactivity index β in D_2O and H_2O.

The σ_{D_2O} value extrapolated at zero LNCs concentration obtained with DPIBF is in really good agreement with the value obtained with RTC in pure D_2O. The values found for σ_{1270} in H_2O and D_2O are similar (see Table 1).

Singlet oxygen is known to be part of the reactive oxygen species (ROS) and oxidizes various kinds of biological molecules such as proteins, lipids, and DNA.[47,48] For instance, in photodynamic therapy, $^1O_2$ is considered as the main cytotoxic species able to induce cell death.[1,2,7] In this context, this study could be of interest in living cells in order to estimate singlet oxygen production for dosimetry and reactivity with specific biotargets. Moreover, LNCs dispersions in D_2O is a heterogeneous medium which can mimic a lipidic membrane environment. The two pseudophases model could be then a first step to understand the dynamic of singlet oxygen in a living cell.

■ ASSOCIATED CONTENT

Supporting Information

Complementary experiments on lipid nanocapsules dispersions and solutions of RTC in D_2O and H_2O. This material is available free of charge via the Internet at http://pubs.acs.org.

■ AUTHOR INFORMATION

Corresponding Author

*E-mail: emmanuel.courtade@univ-lille1.fr.

Notes

The authors declare no competing financial interest.

■ ACKNOWLEDGMENTS

We gratefully acknowledge financial support from the Centre National de Recherche Scientifique (CNRS), the Université Lille 1, and the Région Nord Pas de Calais.

■ REFERENCES

(1) Dougherty, T. J.; Gomer, C. J.; Henderson, B. W.; Jori, G.; Kessel, D.; Koberlik, M.; Moan, J.; Peng, Q. *J. Natl. Cancer. Inst.* **1998**, *90*, 889−905.
(2) Dolmans, D. E.; Fukumura, D.; Jain, R. K. *Nat. Rev.* **2003**, *3*, 380−387.
(3) Ogilby, P. *Chem. Soc. Rev.* **2010**, *39*, 3181−3209.
(4) Aubry, J. M.; Pierlot, C.; Rigaudy, J.; Schmidt, R. *Acc. Chem. Res.* **2003**, *36*, 668−675.
(5) Foote, C. S. *Science* **1968**, *162*, 963−970.
(6) Schweitzer, C.; Schmidt, R. *Chem. Rev.* **2003**, *103*, 1685−1757.
(7) Anquez, F.; Yazidi-Belkoura, I. E.; Randoux, S.; Suret, P.; Courtade, E. *Photochem. Photobiol.* **2012**, *88*, 167−174.
(8) Krasnovsky, A. A. J.; Roumbal, Y. V.; Ivanov, A. V.; Ambartzumian, R. V. *Chem. Phys. Lett.* **2006**, *430*, 260−264.
(9) Krasnovsky, A. A. J.; Ambartzumian, R. V. *Chem. Phys. Lett.* **2004**, *400*, 531−535.
(10) Krasnovsky, A. A. J.; Roumbal, Y. V.; Strizhakov, A. A. *Chem. Phys. Lett.* **2008**, *458*, 195−199.
(11) Krasnovsky, A. A. J.; Kozlov, A. S.; Roumbal, Y. V. *Photochem. Photobiol. Sci.* **2012**, *11*, 988−997.
(12) Sivery, A.; Anquez, F.; Pierlot, C.; Aubry, J.; Courtade, E. *Chem. Phys. Lett.* **2012**, *555*, 252−257.

(13) Barras, A.; Mezzetti, A.; Richard, A.; Lazzaroni, S.; Roux, S.; Melnyk, P.; Betbeder, D.; Monfilliette-Dupont, N. *Int. J. Pharm.* **2009**, *379*, 270−277.
(14) Barras, A.; Boussekey, L.; Courtade, E.; Boukherroub, R. *Nanoscale* **2013**, *5*, 10562−10572.
(15) Amat-Guerri, F.; Lempe, E.; Lissi, E.; Rodrigues, F.; Trull, F. *J. Photochem. Photobiol. A* **1996**, *93*, 49−56.
(16) Rigaudy, J.; Cuong, N. *C. R. Acad. Sci.* **1962**, *254*, 4184−4186.
(17) Nardello, V.; Azaroual, N.; Cervoise, I.; Vermeersch, G.; Aubry, J. M. *Tetrahedron* **1996**, *52*, 2031−2046.
(18) Nardello, V.; Brault, D.; Chavalle, P.; Aubry, J. M. *J. Photochem. Photobiol. B* **1997**, *39*, 146−155.
(19) Nardello, V.; Aubry, J. M. *Tetrahedron Lett.* **1997**, *38*, 7361−7364.
(20) Lee, P. C.; Rodgers, M. A. J. *J. Phys. Chem.* **1983**, *87*, 4894−4898.
(21) Lee, P. C.; Rodgers, M. A. J. *J. Phys. Chem.* **1984**, *88*, 3480−3484.
(22) Borsarelli, C. D.; Durantini, E. N.; Garcia, N. A. *J. Chem. Soc., Perkin Trans.* **1996**, *2*, 2009−2013.
(23) Aubry, J. M.; Bouttemy, S. *J. Am. Chem. Soc.* **1997**, *119*, 5286−5294.
(24) Martinez, L.; Martinez, C. G.; Klopotek, B. B.; Lang, J.; Neuner, A.; Braun, A. M.; Oliveros, E. *J. Photochem. Photobiol. B* **2000**, *58*, 94−107.
(25) Wilkinson, F.; Helman, W. P.; Ross, A. B. *J. Phys. Chem. Ref. Data* **1995**, *663*, 664−911.
(26) Turro, N. J.; Aikawa, M.; Yekta, A. *Chem. Phys. Lett.* **1979**, *64*, 473−478.
(27) Han, P.; Bartels, D. M. *J. Phys. Chem.* **1996**, *100*, 5597−5602.
(28) Ogilby, P. R.; Foote, C. S. *J. Am. Chem. Soc.* **1983**, *105*, 3423−3430.
(29) Skovsen, E.; Snyder, J.; Lambert, J.; Ogilby, P. *J. Phys. Chem. B* **2005**, *109*, 8570−8573.
(30) Heurtault, B.; Saulnier, P.; Pech, B.; Proust, J.; Benoit, J. *Pharm. Res.* **2002**, *19*, 875−880.
(31) Anquez, F.; Suret, P.; Sivery, A.; Courtade, E.; Randoux, S. *Opt. Express.* **2010**, *19*, 22928−22936.
(32) Jensen, R. L.; Arnbjerg, J.; Ogilby, P. R. *J. Am. Chem. Soc.* **2010**, *132*, 8098−8105.
(33) Weiss, R. *Deep-Sea Res.* **1970**, *17*, 721−735.
(34) Battino, R.; Rettich, T. R.; Tominaga, T. *J. Phys. Chem. Ref. Data* **1983**, *12*, 163−178.
(35) Losev, A.; Nichiporovich, I.; Byteva, I.; Drozdov, N.; Jghgami, I. *Chem. Phys. Lett.* **1991**, *181*, 45−50.
(36) Aubry, J.; Rigaudy, J.; Cuong, N. K. *Photochem. Photobiol.* **1981**, *33*, 155−158.
(37) Krasnovsky, A. A. J.; Drozdova, N. N.; Ivanov, A. V.; Ambartzumian, R. V. *Biochemistry (Moscow)* **2003**, *68*, 1178−1182.
(38) Krasnovsky, A. A. J.; Drozdova, N. N.; Roumbal, Y. V.; Ivanov, A. V.; Ambartzumian, R. V. *Chin. Opt. Lett.* **2005**, *3*, S1−S4.
(39) Douzou, P. *Res. Prog. Org. Biol. Med. Chem.* **1972**, *3*, 37−47.
(40) Foote, C. S.; Clennan, E. L. *Active Oxygen in Chemistry*; Blackie Academic and Professional: London, 1995; pp 105−140.
(41) L..Gilbert, D.; Colton, C. A. *Reactive Oxygen Species in Biological Systems: An Interdisciplinary Approach*; Kluwer Academic/Plenum: Norwell, MA, 1999.
(42) Long, C. A.; Kearns, D. R. *J. Am. Chem. Soc.* **1974**, *97*, 2018−2020.
(43) Krasnovsky, A. A. J. *Photochem. Photobiol.* **1979**, *29*, 29−36.
(44) Khan, A.; Kasha, M. *Proc. Natl. Acad. Sci. U.S.A.* **1979**, *76*, 6047−6049.
(45) Ogilby, P. R. *Acc. Chem. Res.* **1999**, *32*, 512−519.
(46) Bromberg, A.; Foote, C. S. *J. Phys. Chem.* **1989**, *93*, 3968−3969.
(47) Cadet, J.; Delatour, T.; Douki, T.; Gasparutto, D.; Pouget, J.-P.; Ravanat, J.-L.; Sauvaigo, S. *Mutat. Res.* **1999**, *424*, 9−21.
(48) Halliwell, B.; Gutteridge, J. M. C. In *Free Radicals in Biology and Medicine.*; Press, C., Ed.; Oxford: UK, 2007.